RSC Advances

ROYAL SOCIETY OF CHEMISTRY

www.rsc.org/advances

Cite this: DOI: 10.1039/c0xx00000x

www.rsc.org/xxxxxx

ARTICLE

Fluorophore-doped calcium phosphate nanoparticles for non-toxic biomedical applications

Anuradha[a], Jagdish Chandra Joshi[b], Kavita Gulati[b], Arunabha Ray[b] and Indrajit Roy[a*]

Received (in XXX, XXX) Xth XXXXXXXXX 20XX, Accepted Xth XXXXXXXXX 20XX

DOI: 10.1039/b000000x

We report the synthesis of optically doped calcium phosphate nanoparticles (CPs), with and without surface coating with the biocompatible polymer chitosan. Trisilanol was used to restrict the size of calcium phosphate in the nano-dimension. The diameter of the nanoparticles was found to be less than 200 nm. Powder X-ray diffraction (XRD) study demonstrated the crystalline nature of the nanoparticles, largely matching with the XRD pattern of hydroxyapatite, which is the most common crystalline form of calcium phosphate. Upon fluorophore encapsulation in these nanoparticles, the optical property of the fluorophore not only remained preserved, but also displayed enhanced stability against chemical quenching in comparison to its free form. *In vitro* analysis showed that these nanoparticles are uptaken by cells, the uptake being enhanced upon coating with chitosan. No sign of *in vitro* cytotoxicity was observed in the dosages tested. Preliminary *in vivo* studies showed that oral administration of these nanoparticles in healthy Wistar rats, in a dose of 2000 mg/kg, did not result in any visible sign of acute toxicity. These results highlight the potential for CPs to be used as safe and efficient agents for optical bioimaging and drug delivery.

Introduction

Over the past few decades, the advent of nanotechnology has ushered several advances in medical techniques. Some of the hallmarks of nanotechnology in medicine are targeted and sustained drug delivery, multimodal bioimaging, non-viral gene delivery, theranostics, etc.[1-5] However, for nanotechnology to make a lasting impact on medicine, it is also important that along with the efficiency, the safety aspects of nanomaterials are also addressed. It is important that the nanoparticles intended for medical applications are non-immunogenic, biocompatible, biodegradable, and do not physically or chemically obstruct essential biological processes.[6] These attributes are likely to be found in nanoparticles composed mainly of normal physiological components, rather than metals, semiconductors, or synthetic polymers.

An extremely promising non-immunogenic, biocompatible and biodegradable material is calcium phosphate, which is a natural component of bone and teeth. This material has gained significant attention in the biomedical community, with applications in prosthetic and dental implants, tissue engineering, and drug delivery.[7-16] Calcium phosphate nanoparticles (CPs), encapsulating therapeutic and/or diagnostic agents, have been synthesized using various techniques, such as nanoprecipitation within microemulsion medium, hydrothermal synthesis, hydrolysis, sol-gel techniques, etc. [17] However, there are concerns related to the colloidal stability of these nanoparticles, which are reflected in their tendency to form aggregates in the physiological milieu. Improperly controlled surface reactivity of calcium phosphate, such as it's tendency to form hydrogen bonds with itself, is thought to be a potential cause of their aggregation. Such aggregation adversely effects their biomedical function. For example, there are conflicting reports about the transfection efficiency of calcium phosphate/DNA nanoplex systems.[18]

Nanoparticle aggregation and other non-specific interactions can be prevented via (a) efficient control of nanoparticle growth during synthesis, and (b) proper post-synthetic modification of their surface. Typically growth of calcium phosphate nanoparticles is modulated via physical interaction with surfactant molecules. However, such interactions are often unstable. More efficient growth control can be achieved using ligands that bind to the nanoparticle surface via coordination bonding. Recently, trisilanols have been recognised as promising ligands with strong coordination ability towards surface of biominerals, such as calcium carbonate and calcium phosphate.[19] Post-synthetic modifications of the nanoparticle surface can be achieved via coating with biocompatible, non-toxic and hydrophilic polymers, such as chitosan (CH).[20, 21] These synthetic and post-synthetic modifications of nanoparticles are crucial factors that modulate their interaction with the biological system.

Herein, we report the synthesis of fluorophore-doped CPs in a methanolic medium, with surface grafted with trisilanol. After synthesis in methanol, the doped nanoparticles were dried, and then transferred to aqueous media, without and with a further coating with chitosan. The synthesized nanoparticles were characterized for various physical properties, using transmission electron microscopy (TEM), powder X-ray diffraction (XRD), Energy-dispersive X-ray spectroscopy (EDX),

Thermogravimetric analysis (TGA), UV-visible spectrophotometry, and spectrofluorimetry. The optical stability of the nanoparticle-encapsulated fluorophore against chemically induced quenching has been evaluated *vis-a-vis* that of the free fluorophore. After characterization, preliminary *in vitro* biological investigations of the nanoparticles were conducted, which included estimating their cellular uptake and non-specific toxicity. Finally, *in vivo* acute toxicity study of these nanoparticles was carried out in Wistar rats following oral administration.

Experimental

Materials:

Calcium chloride, disodium hydrogen phosphate, sodium hydroxide, methanol, tetrahydrofuran (THF) and chitosan (CH) were purchased from SRL (India). Fluorescein isothiocyanato-dextran (FD), Tris-HCl buffer and Triton X-100 were purchased from Sigma-Aldrich (USA). Cell culture media (DMEM), fetal calf serum (FCS), antibiotics (penicillin and streptomycin), amphotericin B, and MTT Reagent [3-(4,5-dimethylthiazol-2-yl)-2,5-diphenyltetrazolium bromide] were obtained from Genetix (India). Human lung cancer A-549 cells were purchased from ATCC (USA).

Synthesis of calcium phosphate nanoparticles:

Trisilanol [$(c\text{-}C_5H_9)_7Si_7O_9(OH)_3$] was prepared according to previously reported method.[22] Sodium hydroxide was added to 45 ml of a methanolic solution of the prepared trisilanol (feed molar ratio of sodium hydroxide to trisilanol was 3:1). After that, to the resulting solution of sodium trisilanolate in methanol, 1.5 ml of each aqueous reactant solutions (0.1 M $CaCl_2$ and 0.035 M Na_2HPO_4), and 80 µl of double distilled water, were added via syringe at 30^{o}C under N_2 atmosphere. For synthesis of fluorescently doped nanoparticles, instead of 80 µl of water, equal volume of an aqueous solution of FD (10 mg/ml) was added to the solution. Appearance of translucency in the solution indicated the formation of nanoparticles. For chitosan coating, an additional 1.4 ml of 0.1% chitosan solution (dissolved in 1% aqueous acetic acid) was added. This solution was kept at 30^{o}C under N_2 atmosphere for 24 hours with gentle stirring for the completion of the reaction. The resulting calcium phosphate nanoparticles (CPs) were separated by centrifugation (10,000 rpm, 5 min), and washed three times with pure methanol. Finally, the precipitate was dried in a vacuum oven at 50^{o}C for one day. The nanoparticles were further purified by suspending the precipitate in THF by vigorous stirring, followed by separation by centrifugation (10,000 rpm, 5 min). Finally, dried nanoparticles were then dispersed in water for further studies.

Characterization:

The sizes of the calcium phosphate nanoparticles were determined using transmission electron microscopy (TEM). Aqueous dispersion of nanoparticles were sonicated, drop-coated and dried onto formvar coated 200 mesh copper grids (Ted Pella, USA), followed by imaging using a TECNAI G2-30 U TWIN TEM instrument (FEI, Eindhoven, The Netherlands), with an acceleration voltage of 300 kV. The same instrumentation setup was used for probing the elemental composition (using energy dispersive x-ray spectroscopy, or EDX) of the nanoparticles.

High resolution powder X-ray diffraction (XRD) was used to analyze the phase composition of the nanoparticles, using a Brukar D8 Discover X-ray spectrometer, over the 2Θ range from 10–70^0, with a step size of 0.02^0, scan rate of 1.5 second/step, 40 milliamp current and 40KV voltage, using Cu-Kα radiation (λ= 1.54060 A°). The fourier transform infrared spectroscopy (FTIR) spectra for the prepared nanoparticles were recorded on Perkin Elmer RX1 Instrument. TGA Spectra of the particles were analysed with Perkin Elmer Instrument. The optical properties (UV-visible absorption and fluorescence emission spectra) of the nanoparticles, with and without encapsulated fluorophore, were recorded using a Shimadzu UV-1601 spectrophotometer (Shimadzu, Kyoto, Japan) and a Cary Eclipse fluorescence spectrometer (Varian, Palo Alto, CA), respectively.

The stability of the fluorophore, both free and nanoencapsulated, was studied using a fluorescence quenching experiment. Here, fixed concentrations of free and nanoencapsulated FD in aqueous medium were treated with various concentrations of the chemical quencher Cu^{2+} (copper sulfate).[23] Fluorescence emission intensities in the absence (I_o) and presence (I) of various quencher concentrations was then measured using the Cary Eclipse fluorescence spectrophotometer. A plot was made with the natural log of (I/I_o) versus quencher concentration [Q]. The slope of the plot correlated directly with the extent of chemical quenching of the fluorophore.

The release profile of the fluorophore from the nanoparticles was next probed. Dried CPs loaded with fluorophore FD were dispersed in 15 ml of phosphate buffer saline (PBS, pH = 7.4) by simple agitation for 2–3 min. Then, 15ml of the FD-doped CP solution was distributed in 5 vials and was kept at 37^{0}C. At predetermined intervals of time the solutions were centrifuged and the supernatant collected. The amount of released FD was determined by measuring the fluorescence intensity of the various supernatant solutions. The corresponding residues (containing nanoparticle-encapsulated FD) were also dispersed in water and analysed for fluorescence.

In vitro studies:

The human lung cancer cells A-549 were grown in DMEM media, supplemented with 10% fetal bovine serum (FBS), 1% antibiotic penicillin/streptomycin, and 1% antifungal Amphotericin B. The cells were maintained at 37 °C and 5% CO_2 in a humidified incubator, using standard cell culture procedures and manufacturer's instructions.

For analyzing cell viability upon treatment with nanoparticles, one day prior to treatment, the cells were trypsinized and resuspended in fresh media. 75,000 cells/1 ml fresh media were added to each well of a sterilized 24-well plate, and transferred back to the incubator for attachment and overnight growth. Next day, to the cells at a confluency of about 50%, aqueous dispersions of the nanoparticles were added, mixed by swirling, and transferred back to the incubator. After two days of incubation, the plate was taken out, and the cells in each well

were washed three times with sterile PBS, and treated with 100 µl of MTT reagent [3-(4,5-dimethylthiazol-2-yl)-2,5-diphenyltetrazolium bromide, (5 mg/ml in PBS)] for 2 hours.[24] The resulting blue-coloured formazan crystals were dissolved in DMSO, and the optical density of this solution was recorded at 570 nm using UV–visible spectrophotometry. The optical density of each solution reflected the viability of the cells in each well. The percentage viability of the treated cells were calculated after comparing their optical density with that of non-treated cells (positive control), the later being arbitrarily assigned 100 % viability. The experiment was carried out in triplicates.

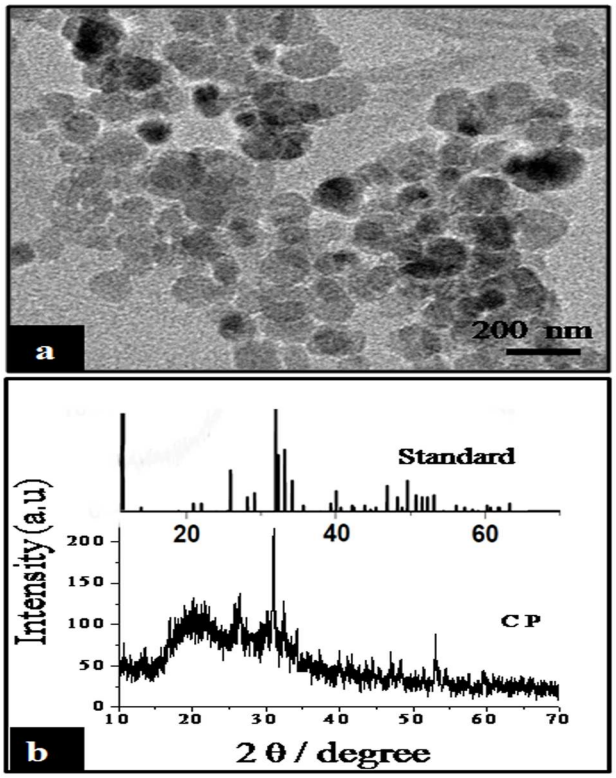

Fig. 1: (a) TEM image of CP, and (b) XRD spectra of CP. The XRD pattern of hydroxyapatite (HA) is provided as a standard.

Fluorescence microscopy of cells and fluorescence estimation from cell lysates were used to monitor the uptake of the fluorophore-doped nanoparticles in cells. One day prior to treatment, the cells were seeded in sterilized 6-well plates (2,00,000 cells/2 ml fresh media in each well) and returned to the incubator. Next day, to the cells at a confluency of about 70%, aqueous dispersion of fluorophore-doped nanoparticles were added (nanoparticle concentration 2.4 µM), mixed by swirling, and returned to the incubator. After two hours of incubation, the plate was taken out, the treatment-media aspirated, and cells in each well washed twice with sterile PBS. The washed cells were fixed by washing with methanol, followed by addition of 50 % glycerol. The fixed cells were then analysed using a fluorescence microscope (ZEISS Axiovert 40 CFL).

The quantitative estimation of uptake of FD-doped CPs in cells via fluorescence analysis of cell lysates was carried out by a similar procedure as above. Here, after nanoparticle treatment and subsequent washing of cells with PBS, as described above, the cells were lysed by adding 200 µl of cell lysis reagent (1 % Triton-X 100 in water) to each well of the 6-well plate, followed by incubation for 30 min with gentle shaking. After this, the cells in the lysis solution were scraped with a sterile scraper, and mixed with an additional 1 ml of PBS added to each well. Then, the mixtures were transferred to microcentrifuge tubes (maximum capacity 1.5 ml). The cell debris was separated from the lysate by centrifugation (3,000 rpm, 5 min). The supernatant (centrifugate) was collected for analysis of FD fluorescence in the spectrofluorimeter.

In vivo toxicity studies:

Female Wistar rats (180-220 g) were used for *in vivo* acute toxicity studies and fed on standard chow diet and water ad libitum. They were acclimatized in experimental laboratory at a constant temperature of 23 ± 2 ^{o}C and were exposed to normal day and light cycle. Animals care was taken as per guidelines in 'Care and use of animals in scientific research' prepared by Indian National Sciences Academy (INSA), New Delhi. The experimental protocol used in the present study was approved by the Institutional Animal Ethical Committee, VP Chest Institute, University of Delhi. For this, the rats were divided into two groups each having five rats - one group acted as vehicle control while the other received CPs. The CPs were dispersed in distilled water and administered orally at the dose of 2000 mg/kg (single dose). After that, these rats were observed daily for 14 days, as per the guidelines of Organisation for Economic Co-operation and Development (OECD). The following parameters were assessed: physical signs like gross animal appearance, salivation, lacrimation, vocalisation, rearings, sedation, and convulsions. Body weight changes were measured by animal weighing balance, motor coordination by Rota rod apparatus and locomotor activity by a Photoactometer (both from INCO, Ambala). Mortality was also noted during the experimental period. The data were analysed by using Student`s t-test and a p value of at least 0.05 was considered as the level of statistical significance.

Results and discussions

The TEM images of the synthesized FD-doped CPs are shown in Fig. 1a. Their diameter varied in the range of 150 and 200 nanometers, with irregular oval shape. Powder XRD patterns of the CP show peaks corresponding to $2\Theta \approx 26^{o}$ (being 002 diffraction, d=3.427) and at $2\Theta \approx 32^{o}$ (overlapping diffraction of 211, d_{211}=2.805). This XRD pattern largely corresponds to that of hydroxyapatite (HA), which is the most common crystalline phase of calcium phosphate (standard JCPDS, #09-0432). The peak at $2\Theta \approx 20^{o}$ appearing in the data is ascribed to trisilanol. No other impurity was observed in the XRD pattern, indicating that the chief inorganic phase of the sample is HA. Overall, the poor crystalline nature of the CP can be ascribed due to low temperature synthetic procedure and chitosan coating.[25]

Result of EDX analysis of the nanoparticles confirms the elemental composition of these nanoparticles, containing carbon, nitrogen, oxygen, silica, phosphorous and calcium. EDX data also show the presence of copper, which is a contamination from the grid (Fig. S1, Supplementary data). The TGA analysis for the

CPs (CP) obtained in the presence of the trisilanol gave a larger weight loss at 250-600 ^{0}C, when compared with that of the pure calcium phosphate, which was due to the decomposition of the organic moieties of the trisilanol (Fig. S2, Supplementary data). [26]

The FTIR spectra of trisilanol, chitosan (CH), CP and CP coated with CH are shown in Fig. 2. The trisilanol spectrum (a) shows signals for Si–O framework (band at 1100 cm^{-1}), together with peaks at 698 and 746 cm^{-1} related to phenyl groups, and signals at 1150 cm^{-1} and 1432 cm^{-1} due to Si-phenyl interaction.[27] In particular, signals in the range 3000–3100 cm^{-1} are relative to C–H on phenyl groups. Bands around 1600 cm^{-1} are related to C-C bonds stretching. [28,29] In CP (b), an additional hump around 1400-1500 cm^{-1} corresponds to the mixing of the trisilanol moiety with the PO_4^{3-} formed during the CP nanoparticle formation. The characteristic FTIR absorption peaks of CP nanoparticles (in the hydroxyapatite form) are evident. The sharp peak around 3450 cm^{-1} was attributed to the stretching vibration of the lattice OH^- ion. [30-32] The presence of PO_4^{3-} is indicated by characteristic bands appearing at 878 and 1095 cm^{-1}. The observation of the asymmetric P-O stretching vibration of the PO_4^{3-} band at 878 cm^{-1} as a distinguishable peak together with sharp peaks around 594 and 698 cm^{-1}corresponds to the O-P-O bending vibration of PO_4^{3-} in hydroxyapatite. Doublet in the range 1000-1100 cm^{-1} was assigned to P-O antisymmetric stretching mode.[33] These bands indicate the characteristic molecular structures of the polyhedrons of PO_4^{3-} in the hydroxyapatite lattice.

FTIR spectrum of CP coated with CH (d) shows that the characteristic peaks of hydroxyapatite CH move apparently upon chemical interaction with each other. The peaks at 1154 cm^{-1} and 625 cm^{-1} (c) relate to the crystallinity of CH.[34] The disappearance of –OH group of hydroxyapatite and the movement of polar groups of CH suggest that the hydroxyl ions on the surface of hydroxyapatite might interact with the plentiful amino and hydroxyl ions of CH via hydrogen bonding.[35-36] Overall, this study confirms that interaction of CH with the nanoparticles.

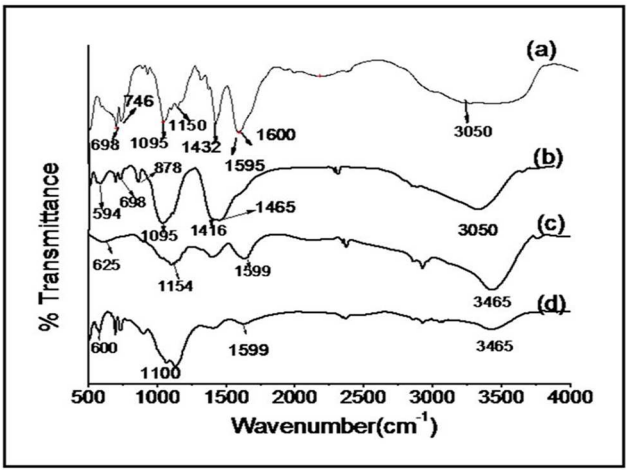

Fig. 2: FTIR spectra of (a) trisilanol only, (b) CP only, (c) chitosan (CH) only, and (d) CPs coated with chitosan (CP-CH).

The optical properties of aqueous solutions of FD and FD encapsulated CP (FD-CP) have been studied by UV-visible and fluorescence spectroscopies; their results are provided in Fig. 3. It was observed that FD, both in the free (FD) and nanoencapsulaed (FD-CP) forms, have an absoaption maxima of 490 nm (Fig. 3a). The observed higher absorbance of CP-CH as compared to CH can be attributed to scattering contribution of the nanoparticles. The fluorescence spectra ($\lambda_{excitation}$ = 490 nm) at normalized absorption shows no discernible difference between the fluorescence positions and intensities of free and CP-encapsulated fluorophore (Fig. 3b). This data shows that the optical properties of the fluorophore are retained in their doped form.

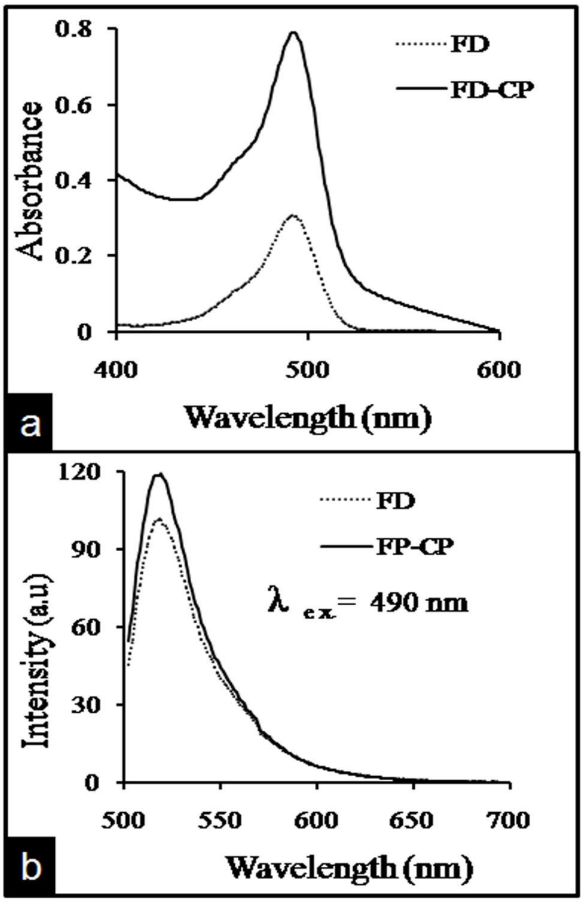

Fig.3: (a) Absorption, and (b) emission spectra of FD and FD-CP.

We further investigated whether nanoencapsulation enhances the stability of the fluorophore FD against chemically-induced fluorescence quenching. From Fig. 4a, it is clear that the free fluorophore is more sensitive to chemical quenching than the nanoencapsulated fluorophore, as evident from the steeper fluorescence quenching curve of the former. However, it is also evident that nanoencapsulation cannot completely prevent the chemical quenching of the fluorophore, but rather provide a relatively enhanced optical stability over the free fluorophore.

Next, we probed the release profile of the fluorophore from the nanoparticles, the results of which are shown in Fig. 4b. The data indicated initial burst release, with about 60% release on the first day, followed by slow release over the next four days, reaching a maxima of about 80 % in five days. This suggests that these nanoparticles can act as drug delivery vehicles; though their release profile needs further optimization via better tuning of their composition.

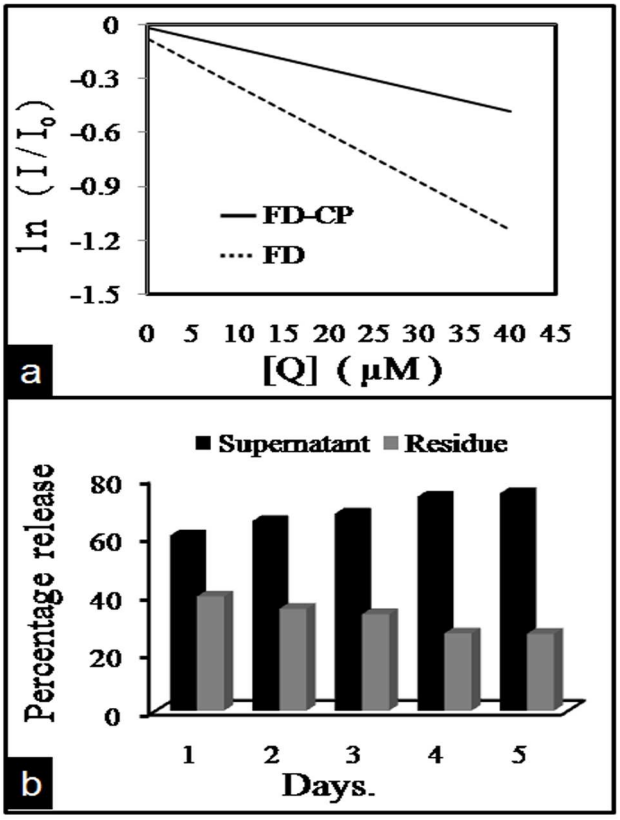

Fig 4. (a) Comparative fluorophore quenching study of FD in free (FD) and nanoencapsulated (FD-CP) form. (b) Release pattern of FD from FD-CP nanoparticles.

Following these characterization studies, we probed the interaction of these nanoparticles with cells *in vitro*, using A-549 cells. First, fluoresecence microscopy results qualitatively demonstrated the uptake of fluorophore-doped nanoparticles in the cells (Fig. S3, Supplementary data). After that, we used spectrofluorimetric analysis of lysates of nanoparticle-treated cells to quantitatively probe the cellular uptake of the nanoparticles. Here, cells were treated with FD-doped CP nanoparticles, with two types of surface properties, i.e. without (FD-CP) and with (FD-CP-CH) chitosan coating. Fig. 5a shows that the cellular uptake of the nanoparticles varied with change in surface property, with the chitosan-coated nanoparticles showing almost four times higher uptake than non-coated nanoparticles. This observation can be explained by the fact that the cationic amino groups present in chitosan helps in favourable interaction of the coated nanoparticles with the outer anionic leaflet of cellular membranes. This interaction results in enhanced cellular uptake via endocytosis.[37] Overall, these above experiments conclude that fluorophore-doped nanoparticles are well uptaken by cells *in vitro*, and extent of which relies on the nanoparticle surface.

Next, in order to study the biocompatibility and non-cytotoxicity of the nanoparticles, we have treated A-549 cells with these nanoparticles (at three different dosages: high, medium and low) for two days, and analyzed the cell viability. It can be seen from Fig. 5b that after 48 hours of nanoparticle-treatment, the cells remained about 80-90 % viable in all the dosages tested, with relatively higher viability for the lower dosages. Moreover, chitosan coating of nanoparticles does not discernibly alter the viability of the treated cells. This data demonstrates that the nanoparticles exert negligible toxic effect on the cells, and can be used in biological applications.

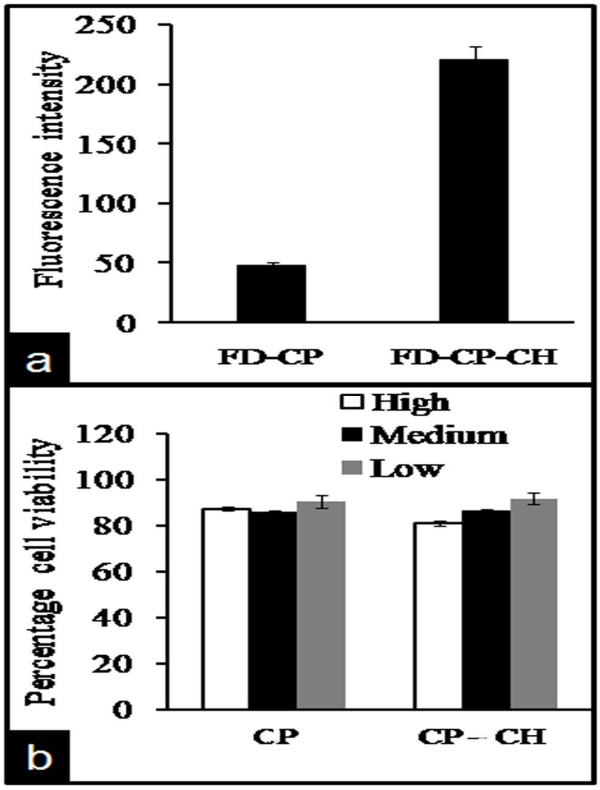

Fig. 5 (a) Quantitative estimation of fluorescence recovered from lysates of cells treated with FD-CP and FD-CP-CH. (b) Cell viability (MTT) assay of CP and CP-CH (High: 100 μg/ml, Medium: 50 μg/ml , Low: 25μg/ml).

Finally, to evaluate the *in vivo* toxicity of these CPs, preliminary experiments were conducted involving oral administration of nanoparticles in healthy rats, as per OECD guidelines. The results of the *in vivo* toxicity studies showed that there were no overt physical signs of toxicity such as stressed animal appearance, salivation, lacrimation, vocalisation, rearings, sedation, or convulsions in CP treated animals. Further, no significant differences were observed in body weight changes, locomotor activity (in photoactometer), and motor coordination (in rota rod) in CP treated group, when compared to vehicle control rats ($p > 0.05$) (Fig. 6; A, B, and C). Further, no mortality was observed during 14 days observation period. Macroscopic examination of vital organs did not show any change in stomach, liver, lungs, heart or ovary in either control or CP-treated groups. This experiment concludes that the nanoparticles are well tolerated by rats following oral administration at a dosage as high as 2,000 mg/kg, upon observation upto two weeks post-treatment. Therefore, these nanoparticles appear to be non-toxic *in vivo* as well. Overall, it can be concluded that these nanoparticles can encapsulate organic fluorophores and provide them with protection from chemical quenching. The use of trisilanol ligands for growth control of nanoparticles during synthesis resulted in their efficient dispersion in aqueous medium. Also, use of

biocompatible trisilanols for growth control obviated the necessity of using harmful surfactants and corrosive solvents during synthesis. These nanoparticles are well uptaken by cells in culture with no sign of toxicity, the uptake being significantly enhanced upon chitosan coating. Finally, we have demonstrated the non-toxicity of these nanoparticles *in vivo* in mice upon oral administration. These results demonstrate the potential of these nanoparticles for safe and efficient imaging and drug delivery applications. More exhaustive *in vivo* toxicity and biodistribution studies are currently underway.

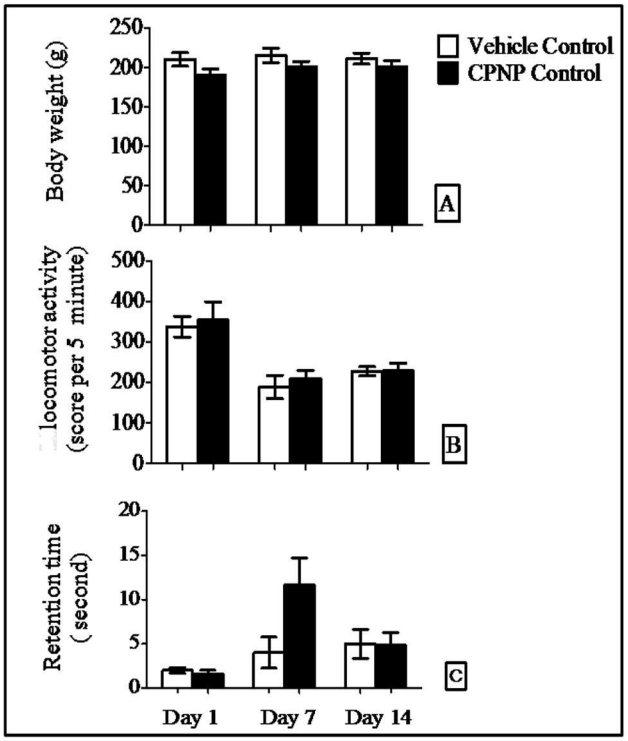

Fig. 6. Acute in vivo toxicity parameters on day 1, 7, and 14 after oral administration of vehicle and CP (CP) in rats. A) Body weight; B) Locomotor activity in Photoactometer; C) Retention time in second on Rota Rod.

Acknowledgements

We are grateful to the Department of Biotechnology (DBT), Government of India, for providing financial support to this study in the form of a research grant (Rapid Grant for Young Investigator 2011-14).

Notes and references

***a**: Department of Chemistry, University of Delhi, Delhi-110007, India. * Tel: +91-9560721851; E-mail: indrajitroy11@gmail.com*
***b**: Department of Pharmacology, VP Chest Institute, University of Delhi, Delhi-110007, India.*

† Electronic Supplementary Information (ESI) available: EDX, TGA, and fluorescence microscopy data. See DOI: 10.1039/b000000x/

1. A. H. Faraji and P. Wipf, *Bioorg. & Med. Chem*., 2009, **17**, 2950.
2. H. Gleiter, *Acta. Mater*., 2000, **48**, 1.
3. H. S. Nalwa (Ed.), Handbook of Nanostructured Materials and Nanotechnology: *New York (2000)*.
4. A.S. Edelstein and RC. Carnmarata (Eds.), 'Nano Materials' Synthesis, Properties and Applications, *Institute of Physics*: *Bristol (1998)*.
5. R. W. Siegel, *Mater. Sci. Eng. B.,* 1993, **19**, 37.
6. S. V. Dorozhkin and M. Epple, *Angew. Chem. Int. Ed..,* 2002, **41**, 3130
7. C. P. Nunes, S. J. Simske, R. Sachdeya, and L. M. Wolford, *J. Biomed. Mater. Res.,* 1997, **36**, 560.
8. R. W. Nicholas and T. A. Lange, *J. Clin. Orthop.,* 1994, **306**, 197.
9. J. C. Elliott, Structure and Chemistry of the Apatites and Other Calcium Orthophosphates. *Elsevier: Amsterdam (1994)*.
10. M. Spector, *J. Clin. Plast. Surg., 1*994, **21**, 437 .
11. S. Bisht, D. Chattopadhyay, and A. Maitra, *J. Biomed. Nanotechnol.,* 2006, **2**, 229.
12. H. T. Schmidt, M. Kroczynski, J. Maddox, Y. Chen, R. Josephs, and A. E. Ostafin, *J. Microencapsulation,* 2006, **23**, 769 .
13. I. Roy, S. Mitra, A. Maitra, and S. Mozumdar, *Int. J. Pharm.,* 2003, **25**, 250.
14. A. Maitra, *Expert Rev. Mol. Diagn.,* 2005, **5**, 893.
15. S. Bisht, G. Bhakta, S. Mitra, and A. Maitra, *Int. J. Pharm.,* 2005, **157**, 288.
16. T. C. Yih and M. Al-Fandi, *J. Cell. Biochem.,* 2006, **97**, 1184.
17. A. Bianco, I. Cacciotti, M. Lombardi, and L. Montanaro, *J. Therm. Anal. Cal.,* 2007, **88**, 237.
18. R. H. Simon, J. F. Engelhardt, Y. Yang, M. Zepeda, S. Weber-Pendelton, M. J. Grossman, and M. Wilson, *Human Gene Ther.,* 1993, **4**, 771.
19. D. K. Keum, K. M. Kim, K. Naka, and Y. Chujo , *J. Mater. Chem.,* 2002, **12**, 2449.
20. L. Chronopoulou, M. Massimi, M. F. Giardi, C. Cametti, L. C. Devirgiliis, M. Dentini, C. Palocci. *Coll. Surf. B: Biointerfaces,* 2013, **103**, 310.
21. V. Uskoković and T. A. Desai. *J. Pharm. Sci.,* 2014, **103**, 567.
22. F. J. Feher, T. A. Budzichowski, R. L. Blanski, K. J. Weller, and J. W. Ziller, *Organometallics,* 1991, **10**, 2526 .
23. B. L. Bales and M. Almgren, *J. Phys. Chem.,* 1995, **99**, 15153.
24. I. Roy, T. Y. Ohulchanskyy, H. E. Pudavar, E. J. Bergey, A. R. Oseroff, J. Morgan, T. J. Dougherty, and P. N. Prasad, *J. Am. Chem. Soc.,* 2003, **125**, 7860.
25. J. Panyam and V. Labhasetwar, *Adv. Drug Deliv. Rev.,* 2003, **55**, 329.
26. L. Wang, I. Sondi, and E. Matijevie, *J. Colloid Interface Sci.,* 1991, **218**, 545.
27. D. Lin-Vien, N. B. Colthup, W. G. Fateley, and J. G. Grasselli, The Handbook of Infrared and Raman Characteristics Frequency of Organic Molecules, *Academic Press Inc., San Diego: CA (1991*).
28. P.C. Eklund, J.M. Golden, and R.A. Jishi, *Carbon,* 1995, **33**, 959.
29. A. Galvez, N. Herlin-Boime, C. Reynaud, C. Clinard, and J.N. Rouzaud., *Carbon,* 2002, **40**, 2775.
30. P. Zimmer and J. Kreuter, *Adv. Drug Deliv. Rev.,* 1995, **6**, 61.
31. D. H. W. Hubert, M. Jung, P. M. Frederik, P. H. H. Bomans, J. Meuldijk, and A. L. German, *Adv. Mater.,* 2000, **12**, 1286.
32. H. P. Hentze, S. R. Raghavan, C. A. McKelvey, and E. W. Kaler, *Langmuir,* 2003, **19**, 1069.

33. Z.Gen-Tao, Y. Qi-Zhi, N.Y. Jie, and J. Gu, *Am. Mineral.*, 2009, **94**, 293.
34. M. Miya, R. Iwamoto, and S. Mima, *J. Polym. Sci. Polym. Phys.,* 1984, **22**, 1149.
35. K. Masanori, I. Toshiyuki, I. Soichiro, N. Hiroko, K. Yoshihisa, T. Kazuo, S. Kenichi, and T. Junzo, *Composite Sci. Technol.,* 2000, **64**, 819 .
36. C. Xianmiao, L .Yubao , Z. Yi, Z . Li, L. Jidong, and W .Huanan, *Mater. Sci. Eng. C.***,** 2009, **29**,29.
37. K. Corsi, F. Chellat, L. Yahia, and J. C. Fernandes, *Biomaterials,* 2003*,* **24**, 1255.